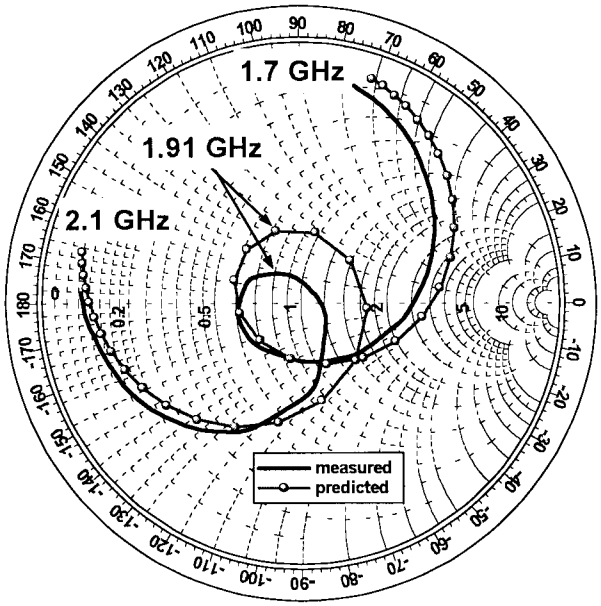

Fig. 2. Predicted and measured impedance of the annular-loaded shorted microstrip patch ($\varepsilon_r = 1.13, \tan\delta = 0.001, d = 5.0$ mm, $R = 11.8$ mm, $x_p = 8.0$ mm, $y_p = 0$, $x_{ps} = 9.3$ mm, $y_{ps} = 0, r_o = 0.325$ mm, $r_{os} = 0.325$ mm, $a = 31.5$ mm, $b = 17.0$ mm).

seen from these results very good agreement between experiment and theory was achieved. The predicted and measured 10-dB return loss bandwidths were 6.6% and 6.8%, respectively. It should be noted that to fabricate the antenna, the shorted patch and ring conductors were etched on 0.254-mm thick *Rogers 5880 Duroid*, which was adhered to one side of the foam with a brass plate affixed to the other to provide a ground plane. The electrically thin *Duroid* layer was not considered when designing the antenna and may be the contributing factor to the minor frequency shift between the measured and analytic results (approximately 1%) as well as the slight closure of the resonant loop. The copolar and cross-polar patterns in the cardinal planes of the shorted patch with a concentric ring were measured and the results were very similar to a conventional microstrip patch antenna mounted on foam. The measured 3-dB beamwidth in the E and H planes were 84° and 75°, respectively, compared to the predicted values of 86° and 70°. The measured H-lane cross-polarization level was always more than 20-dB below the copolar level.

To put these results into perspective, it is useful to compare the theoretical characteristics of the novel patch configuration to both the conventional circular microstrip patch and a shorted patch fabricated using the same substrate. Table I presents the impedance bandwidth, gain, and physical size of the three antennas. As can be seen from these results, the shorted patch with an annular ring has enhanced bandwidth compared to the other patches and is smaller than the conventional patch.

IV. Conclusion

An annular ring loaded probe-fed circular microstrip patch antenna with a shorting pin has been analyzed, fabricated, and measured. The performance of the antenna was accurately predicted using a rigorous full-wave analysis. The novel parasitically coupled microstrip patch with a single shorting pin is smaller in size and has greater bandwidth than a conventional circular microstrip patch antenna examined on the same substrate. Thus, this printed antenna is suitable for applications where limited antenna real estate is available and bandwidth is at a premium.

TABLE I
Comparison of the Characteristics of a Conventional Circular Microstrip Patch, a Shorted Circular Microstrip Patch, and the Proposed Printed Antenna Mounted on the Same Substrate ($d = 5$ mm, $\varepsilon_r = 1.13$)

Printed Antenna Type	10 dB Return Loss Bandwidth	Gain (dBi)	Area (cm^2)
Conventional Circular Patch	4.2%	9.4	51.5
Shorted Circular Patch	2.1%	4.0	4.3
Proposed Printed Antenna	6.6%	8.4	31.2

References

[1] R. Waterhouse, "Small microstrip patch," *Electron. Lett.*, vol. 31, no. 8, pp. 604–605, 1995.
[2] Z. Nie, W. C. Chew, and Y. T. Lo, "Analysis of the annular-ring-loaded circular disk microstrip antenna," *IEEE Trans. Antennas Propagat.*, vol. 38, pp. 806–813, June 1990.

On the Optimal Design of the PML Absorbing Boundary Condition for the FDTD Code

Gianluca Lazzi and Om P. Gandhi

***Abstract*—In this letter, an analytical method to predict and optimize the performance of Berenger's perfectly matched layer (PML) absorbing boundary condition (ABC) for finite-difference time-domain (FDTD) simulations is described. The shape of the conductivity in the PML layers has to be chosen carefully to obtain the best performance for a given number of layers. The relative error is shown to be the composite of two distinct effects: the theoretical reflection coefficient given by the PML layers backed by a metal plane and the second-order error in the differential intrinsic in the FDTD formulation. A theoretical expression to evaluate this error as a function of the number of PML layers and the shape of the conductivity is given, and the result is compared to that obtained for several FDTD test cases. The good agreement of the shapes of the theoretical and numerically derived curves allows the use of the theoretical formulation to optimize the PML region as a function of the shape of the conductivity, resolution, and number of layers.**

***Index Terms*—FDTD methods.**

An independent version of the Berenger's perfectly matched layer (PML) boundary condition [1] was implemented in a finite-difference time-domain (FDTD) code. The shape of the conductivity for the PML layers was chosen similar to [1], but with values obtained from the following formula

$$\sigma_i = \sigma_0 \frac{i^{n+1} - (i-1)^{n+1}}{n+1} \tag{1}$$

Manuscript received March 28, 1996; revised April 9, 1996.

The authors are with the Department of Electrical Engineering, University of Utah, Salt Lake City, UT 84112 USA.

Publisher Item Identifier S 0018-926X(97)02507-6.

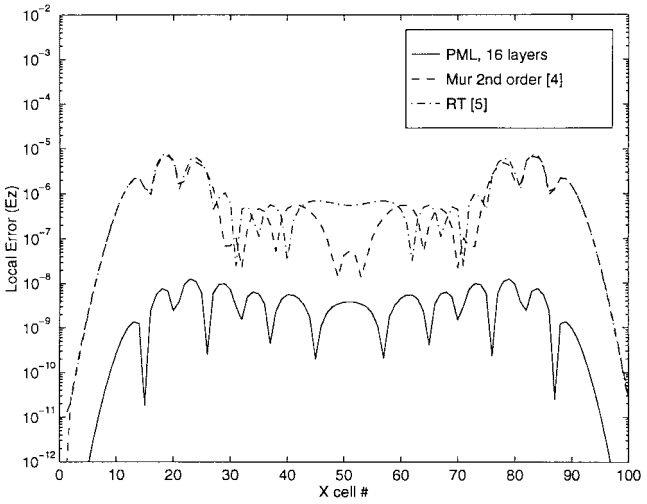

Fig. 1. The local error at the outer boundary of the z component of the electric field for the test case presented in [1] and [2] obtained with the use of three different boundary conditions: 16-layer PML, RT, and Mur second order.

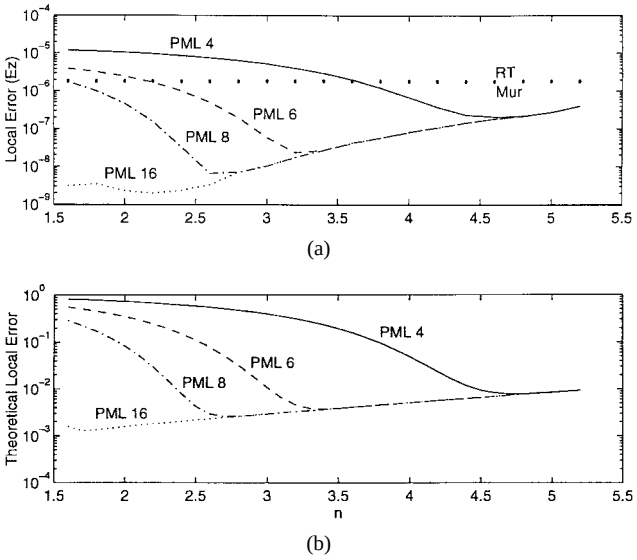

Fig. 2. (a) Average of the local error of the z component of the electric field at the outer boundary of a 50 × 50 × 50 mesh considered for the Hertzian dipole test case as a function of the order n of variation of the shape of the conductivity for all of the considered boundary conditions (PML, RT, Mur). (b) The numerically computed curves for the estimation of the best order n for the various PML boundaries.

where i is the cell number in the PML layer $(i \geq 1)$ and n is the order of variation of the shape of the conductivity.

First, to verify the accuracy of our PML boundary, the same test case presented in [2] and [3] was considered. The local error obtained in a vacuum space of 100 × 50 × 100 cubical cells terminated with a 16-layer PML is compared with that obtained by the use of Mur second-order boundary condition [4]. As a new feature, the local error obtained with the retarded time (RT) boundary condition [5] for the same test case is also considered. A pulse source centered in the vacuum space for 100 time steps of simulation was considered exactly as prescribed in [2]. Fig. 1 confirms the results presented in [3]. Furthermore, it is shown that the RT absorbing boundary condition (ABC) gives similar results to those obtained with Mur second-order, both characterized by a local error considerably higher than that for the 16-layer PML. The effects of varying the number of PML layers, as well as the order of variation of the shape of the conductivity, were investigated. For this test case, we considered the use of four, six, eight, and sixteen layers of PML with various orders n between 1.6 and 3.4. Even the thinnest PML boundary (four layers) for a certain range of n, gave results one order of magnitude more accurate than those obtained with Mur and RT boundaries.

To better present the theory introduced in this paper, a Hertzian dipole sinusoidally excited with electric field amplitude of 0.1 V/m at a frequency of 835 MHz and placed in the center of a 50 × 50 × 50 cells grid of resolution 2 × 2 × 3 mm was considered. Similar to the previous test case, a bigger mesh, i.e., such that the boundaries cannot be reached by the field, was considered, and the simulation run for 120 time steps, with $\Delta t = \delta/(2c_0)$ where $\delta = 2$ mm and c_0 is the speed of the light in vacuum. The average of the local error on the border line of the mesh is plotted in Fig. 2(a) for the various boundaries and different values of the order n for the conductivity $(1.6 \leq n \leq 5.2)$. It is interesting to observe that even though the grid resolution is extremely high, it is possible even with a four-layer PML to improve the performance by more than one order of magnitude relative to Mur and RT ABC's. Furthermore, as can be seen, depending on the number of layers used for the PML, the best performance of the boundary can be achieved within a small range of n: both lower values and higher values for n gave nonoptimal boundary performance. This can be explained observing that the error can be considered to be the composite of two distinct effects: the theoretical reflection coefficient given by the PML layers backed by a metal plane and the second-order error in the differential intrinsic in the FDTD formulation. The first effect is dominant for low values of n, while the second one is dominant for high values of n. To obtain a more convenient pseudoanalytical formulation, we will consider the continuous form of (1)

$$\sigma(x) = \sigma_0 \frac{\left(\frac{x}{\delta}+1\right)^{n+1} - \left(\frac{x}{\delta}\right)^{n+1}}{n+1}. \tag{2}$$

where δ is the cell size considered for the PML layers.

The theoretical reflection coefficient due to a PML layer with σ given by (2) is, therefore

$$R = e^{-2Z_0 \int_{0.5\delta}^{(m-0.5)\delta} \sigma(x)dx} \tag{3}$$

with Z_0 being the intrinsic impedance of vacuum and m the number of PML layers.

With respect to [1, (34)], the limits of the integral are set, respectively, to 0.5δ and $(m - 0.5)\ \delta$, giving the possibility to obtain, with (3), a reflection coefficient closer to that one would obtain considering the stair-step approximation of the shape of the conductivity in accordance with (1).

The error intrinsic in the FDTD formulation is instead proportional to a factor $(\delta/2)^2/6$ to the third derivative of the field. This error should be integrated over x to obtain the overall contribution of the PML layer

$$|E_{\mathrm{FDTD}}| = \frac{(\delta/2)^2}{6} \int_{0.5\delta}^{(m-0.5)\delta} \frac{\partial^3}{\partial x^3} e^{-Z_0\sigma(x)x}\, dx \tag{4}$$

where, again, the integral limits are chosen for a better matching with the stair-step approximation actually used in the FDTD.

For the composite error due to the presence of the PML boundary, we can write therefore

$$E = R + |E_{\mathrm{FDTD}}|. \tag{5}$$

In Fig. 2(b), (5) is plotted as a function of n for the various PML thicknesses. As can be seen, the families of curves plotted in Fig. 2(b) reproduce in the shape very well the curves obtained for the dipole test case. Particularly, it should be noticed as the best value of n for

each PML boundary can be predicted extremely well with the use of the theoretical curves. The ordinate axes of Fig. 2(a) and (b) are different in values due to the fact that Fig. 2(a) gives a relative error that, therefore, depends upon the intensity of the source, distance of observed points from the source, and the monitored quantity (in this case, E_z).

Furthermore, the error obtained by (4) is likely to be overestimated, having considered a maximum source of error by means of the only first term of the series that should be considered to evaluate the overall error contribution of every single cell, and considering the error of all the layers given simply by a sum of maximum errors. Moreover, the theoretical effect is relative to a single-dimensional problem, instead of the three-dimensional results presented in Fig. 2(a) that are likely to have a better behavior allowing any of the reflected waves the possibility to be absorbed by intervening PML layers. The same analysis was also performed using, instead of the integral, a more correct expression that should consider a series of discrete contributions due to every single layer. In such a case, (3) and (4) become

$$R = e^{-2Z_0\delta\sum_{i=1}^{m}\sigma_i} \tag{6}$$

$$|E_{\mathrm{FDTD}}| = \frac{(\delta/2)^2}{6}\delta\sum_{l}^{m} Z_0^3\sigma_i^3 e^{-Z_0\sigma_i i\delta} \tag{7}$$

and we obtained curves almost identical to those reported in Fig. 2(b).

Several other test cases were also tried, and a similar agreement was always observed. The importance of this approach is extreme in predicting the best order of variation for the shape of the conductivity to design a PML layer to be used as the ABC in FDTD codes. Moreover, as can be deduced from (3) and (4), the relative errors are not functions of frequency, but only of the cell size and the number of PML layers. Therefore, a class of universal curves could be derived having as variables the order n, the number of PML layers, and the grid cell size.

ACKNOWLEDGMENT

The authors would like to thank Y. Cui for his contribution of the code preparation and C. M. Furse for helpful suggestions.

REFERENCES

[1] J. P. Berenger, "A perfect matched layer for the absorption of electromagnetic waves," *J. Computat. Phys.*, vol. 114, pp. 185–200, 1994.

[2] T. G. Moore, J. G. Blashak, A. Taflove, and G. A. Kriegsmann, "Theory and applications of radiation boundary operators," *IEEE Trans. Antennas Propagat.*, vol. 36, pp. 1797–1812, Dec. 1988.

[3] D. S. Katz, E. T. Thiele, and A. Taflove, "Validation and extension to three dimensions of the berenger PML absorbing boundary condition for FD-TD meshes," *IEEE Microwave Guided Wave Lett.*, vol. 4, pp. 268–270, Aug. 1994.

[4] G. Mur, "Absorbing boundary conditions for the finite-difference approximation of the time-domain electromagnetic-field equations," *IEEE Trans. Electromagn. Compat.*, vol. 23, pp. 377–382, Nov. 1981.

[5] S. Berntsen and S. N. Hornsleth, "Retarded time absorbing boundary conditions," *IEEE Trans. Antennas Propagat.*, vol. 42, pp. 1059–1064, Aug. 1994.